Evidence of the Interaction of Evaporated Pt Nanoparticles with Variously Treated Surfaces of Highly Oriented Pyrolytic Graphite

D-Q. Yang, G.-X. Zhang, and E. Sacher*

Regroupement Québécois de Matériaux de Point, Département de Génie Physique, École Polytechnique, C.P. 6079, succursale Centre-Ville, Montréal, Québec H3C 3A7, Canada

M. José-Yacamán and N. Elizondo†

Center for Nano and Molecular Technology, Texas Materials Institute, Department of Chemical Engineering, The University of Texas at Austin, Austin, Texas 78712

Received: January 24, 2006; In Final Form: March 8, 2006

The interactions of Pt nanoparticles, deposited by evaporation onto highly oriented pyrolytic graphite surfaces modified by kiloelectronvolt Ar^+ beam treatment, have been studied by X-ray photoelectron spectroscopy core-level line shape analysis. The C1s and $Pt4f_{7/2}$ peaks were each considered to be composed of one asymmetric peak, and changes in their asymmetry parameters were used to study their interfacial interactions. In addition to these changes, strong signal intensity changes with time were found for both the C1s and Pt4f peaks, indicating an initial crystalline orientational instability of the Pt nanoparticles, which is supported by time-dependent high-resolution electron microscopy studies at elevated temperatures.

Introduction

The interaction between metal nanoparticles and substrate surfaces has long attracted attention.[1−3] This is because of underlying interests in understanding (1) the behavioral transition from atomic to bulklike properties, as a function of nanoparticle size, (2) the effect of size-dependent electronic structures in heterogeneous catalysis, (3) the dimensionally controlled fabrication of supported nanoparticles, (4) thin film deposition onto heterogeneous surfaces,[4] and (5) the adhesion associated with interfacial interactions.

Pt nanoparticles, one of the most important catalysts in the petroleum reforming and petrochemical industries, as well as in fuel cells, are of considerable interest, especially when supported on carbonaceous materials, such as amorphous carbon and graphite.[1,5−17] Studies have indicated that the evaporation, sputter, and electrochemical depositions of Pt all lead to particle formation on such substrates, due to both a lack of substrate wetting and relatively weak interfacial interactions.[10,13]

X-ray photoelectron spectroscopy (XPS) is a major tool in the characterization of the chemical and electronic structural properties of nanoparticles, and has been extensively used to characterize Pt nanoparticles supported on highly oriented pyrolytic graphite (HOPG) or amorphous carbon (a-C).[5−17] The main conclusions of these studies were that (1) the core-level Pt4f spectrum shifts to high binding energy with decreasing particle size,[7−17] (2) the full width at half-maximum (fwhm) of the core level decreases with increasing particle size,[7,8,12] similar to the behaviors of other supported nanoparticles, e.g., Cu on HOPG,[18,19] and (3) the asymmetries of both the $Pt4f_{7/2}$ and $Pt4f_{5/2}$ components increase with increasing nanoparticles size,[7,8,12,20] to a maximum for bulk Pt. We emphasize that this is opposite the behaviors of first transition series metals, e.g., Ni, Mn, Cr, V, Cu, etc.[2,21]

In disagreement, a recent study, by Fauth et al.,[15,16] suggested that the Pt XPS shift is a result of interfacial interaction between Pt and defects on the graphite surface, consistent with Pt clusters supported on a Ag surface,[22] rather than from any Pt particle size effects. In their view, the size-dependent behavior of Pt nanoparticles may not play an important role in the core-level binding energy shift.

The treatment of asymmetric XPS peaks as single asymmetric peaks, rather than as an asymmetric composite of several symmetric peaks, has a long history. In 1967, Mahan[23] proposed that the conduction electron scattering amplitude, for interband absorption or emission at the metal Fermi level, is a singularity. Subsequently, in the third of a series of papers on singularities in metals, Nozières and de Domenicis[24] showed that this singularity arose because of the competition between the scattering resonance and deep-level broadening. Doniach and Šunjic[25] and, later, Gadzuk and Šunjic[26] demonstrated that, when the Mahan proposal was applied to photoelectron emission from metals, an asymmetry was expected in the metal core-level electron emission peak, extending to the lower kinetic (i.e., higher binding) energy side. The reason for this is a potential created between the hole formed by the photoemission and the remaining electrons; this permits the promotion of electrons near the Fermi level to empty states just above it. As in a shake-up process, this promotion occurs simultaneously with photoemission, and indeed, Gadzuk and Šunjic[26] referred to this as the Mahan shake-up structure. The equation that Doniach and Šunjic[25] derived for the photoemission line shape intensity, I, is

$$I(\epsilon) = \frac{\Gamma(1-\alpha)}{(\epsilon^2+\gamma^2)^{(1-\alpha)/2}}\left[\frac{\cos \pi\alpha}{2} + (1-\alpha)\tan^{-1}\frac{\epsilon}{\gamma}\right] \quad (1)$$

where Γ is the gamma function, ϵ is the energy relative to that

* To whom correspondence should be addressed. Phone: (514) 340-4711, ext 4858. Fax: (514) 340-3218. E-mail: edward.sacher@polymtl.ca.
† On leave from the Universidad Autonoma of Nuevo Léon, Mexico.

10.1021/jp060513d CCC: $33.50
Published on Web 04/06/2006

at the peak height of the unbroadened line, γ is the lifetime width of the hole, and α is the Anderson asymmetry parameter,[27] given as

$$\alpha = 2\sum_{l}(2l+1)[\delta_l/\pi]^2 \qquad (2)$$

Here, δ_l is the Fermi-level phase shift of the lth partial wave. Because the calculation of α is formidable, the practice has been to turn the problem around and evaluate α from the asymmetry. Confirmation has, thus, been based on consistency (e.g., between spin−orbit components) and interlaboratory reproducibility. The end result is the following: despite inconsistencies of α values for spin−orbit components,[28,29] and experimental data that have been used both pro[30] and con,[31] there is a general concurrence that both experiment[32−39] and theory[40] support the Mahan singularity as the source of the asymmetry.

Because of this, it has since been generally assumed that any asymmetric XPS core emission peak, particularly for metals, is due to the Mahan shake-up process. However, we have recently shown[18,19] that the asymmetry in the C1s peak of HOPG is due, instead, to the existence of identifiable carbon species. Further, in an as yet unpublished study,[41] a Co film was found to initially display symmetric 2p spin−orbit components, which became increasingly asymmetric with time under vacuum; simultaneously, a peak appeared at 283 eV in the C1s spectrum, indicative of carbide formation,[42] which increased in magnitude with increasing Co2p asymmetry.

We have considered the applicability of the Mahan theory to the metal nanoparticles we have been studying. In a recent examination of Ni nanoparticle deposition onto HOPG,[21] we found that the asymmetry of the Ni2p spin−orbit components decreased with increasing nanoparticle size. This was found to be due to the presence of two overlapping symmetric peaks, the first being due to the presence of Ni^0. The second, at a binding energy slightly higher than that of the Ni^0 peak, was due to those Ni atoms in the nanoparticle directly bonded to surface defects on the HOPG. The asymmetry decreased with increasing nanoparticle size because the deposited Ni atoms added to the existing nanoparticles in the absence of further surface defects, raising the intensity of the Ni^0 peak, alone. Similar results have been obtained for Cu nanoparticles supported on both HOPG and low-permittivity polymers.[43]

Further, in a recent paper on peak deconvolution techniques,[44] comparing (1) one single asymmetric peak and (2) several overlapping symmetric peak components, we demonstrated that the single-peak asymmetry of the C1s spectrum of HOPG is due to the increase in intensity of that symmetric peak component signaling structural damage.

Here, we consider Pt nanoparticles evaporated onto three different HOPG surfaces: one of very low defect density (untreated), one of high defect density (Ar^+-treated), and one containing a high defect density of oxidized C structures (Ar^+ treatment, followed by air exposure). We use XPS peak shape analysis to explore the interactions between the Pt nanoparticles and the HOPG surface, concentrating our attention on the asymmetry changes of the C1s and $Pt4f_{7/2}$ spectra induced by Pt deposition.

Experimental Section

HOPG, grade ZYA, 1 cm × 1 cm × 2 mm, was obtained from Advanced Ceramics. Inc. It was cleaved with adhesive tape just prior to each experiment and immediately inserted into the X-ray photoelectron spectrometer. Sample surface treatments and Pt deposition were carried out in the UHV preparation chamber of the XPS instrument, which was connected to the analysis chamber by a gate valve. The Ar^+ treatment of HOPG was performed using a 3 keV Ar^+ beam having a flux of $\sim 1 \times 10^{13}$ (ions/cm^2)/s, for 4 min, at an angle of ~60° between the surface normal and the beam. This condition provides a uniform, repeatable surface defect density, as previously shown.[18,19] For surface oxidation, the HOPG was first treated with Ar^+ for 4 min, followed by exposure to air (40% RH at room temperature) for at least 2 h. This exposure has been shown to be sufficient for the free radicals produced at the HOPG surface to react with components in air (O_2, H_2O), to produce oxidation products (−C−OH, −C═O, −COOH).

Pt evaporation was carried out, at room temperature, in the preparation chamber, using a Quad-EVC evaporator (Mantis Deposition, Ltd.) at a rate of ~0.15 nm/min. The thickness was monitored by a quartz crystal microbalance placed near the sample.

XPS was performed in a VG ESCALAB, using nonmonochromated Mg Kα radiation, at 300 W. High-resolution spectra were obtained at a perpendicular takeoff angle, using a pass energy of 20 and 0.05 eV steps. The instrument resolution was ~0.75 eV. After Shirley background subtraction, the peaks were fit using the freely available XPSPeak 4.1 program[45] for asymmetric peak line shapes, which gives the asymmetry in terms of the TS peak shape asymmetry and the TL tail extension asymmetry indices; we have recently shown[44] that an increase in TS reflects any reduced delocalization of electrons in the C1s HOPG π-orbital system, and an increase in TL reflects any subsequent oxidation occurring on air exposure. As shown in our previous paper,[44] α asymmetry indices, calculated from half-widths at half-heights, vary in a fashion identical to that of the XPSPeak TS values, and may be used interchangeably; the use of α is preferred by most workers. We give examples of the use of both.

High-resolution transmission microscopy studies were carried out on a JEOL 2010 FEG instrument, outfitted with a JEOL drift-controlled heating stage, and having an information limit of 0.14 nm. Samples were evaporated onto thin graphene layers that were stripped by adhesive tape from freshly cleaved HOPG and transported to the electron microscope in capsules, under argon; these samples, thin enough to be directly observed in the microscope, were observed at the optimum defocus condition. Experiments were carried out at 450 °C, on the stabilized heating stage; sequential exposures were obtained at 5 s intervals, using a CCD camera.

Results

The C1s spectral envelopes of the samples considered here are asymmetric; they were previously separated into five symmetric components,[18,19] comprising peaks attributed to extensive (undamaged) and localized (damaged) electron delocalization (called C1 and C2, respectively), their $\pi^* \leftarrow \pi$ shake-up satellites (C4 and C5, respectively), and sp^3 defects (C3). It has been found that the C1s spectra do not change significantly on the deposition of many metals,[18,19,46,47] and no new peaks, which would signify carbide formation, appear in the 282−284 eV region. Thus, it is clear that the C1s line shape is insensitive to the presence (i.e., interfacial interaction) of numerous metals. Many researchers[48−53] have found that the asymmetric C1s spectral line shape is well described by the Doniach−Šunjic equation.[25] On the basis of this, it has generally been supposed that the C1s line shape of HOPG is determined

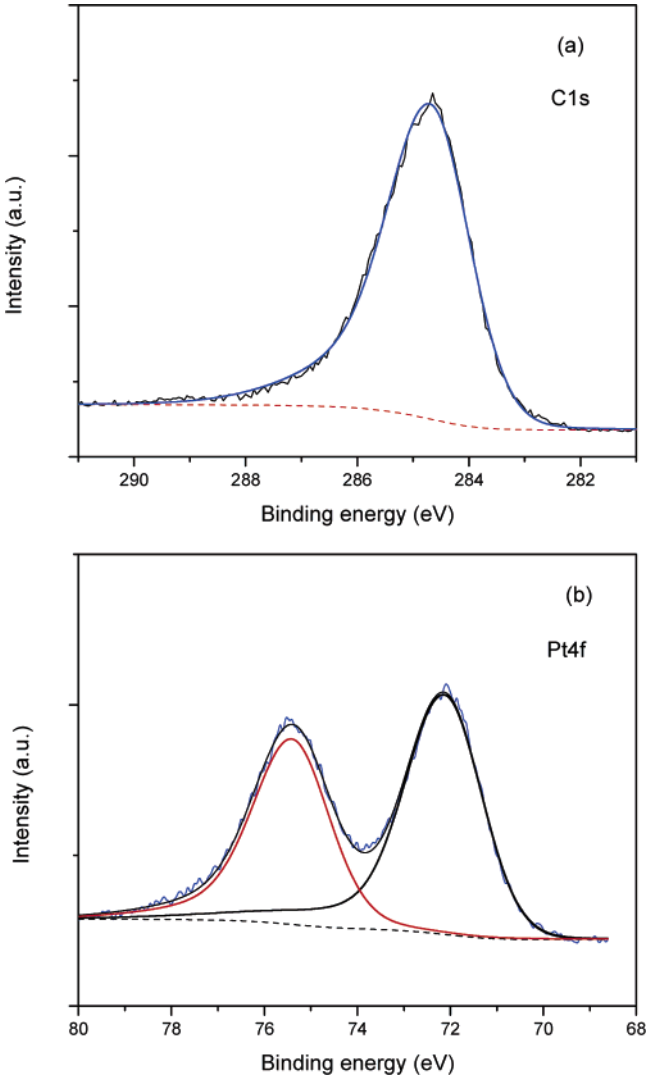

Figure 1. XPS spectra of 0.2 nm Pt evaporated onto the Ar^+-treated HOPG surface: (a) C1s, (b) Pt 4f.

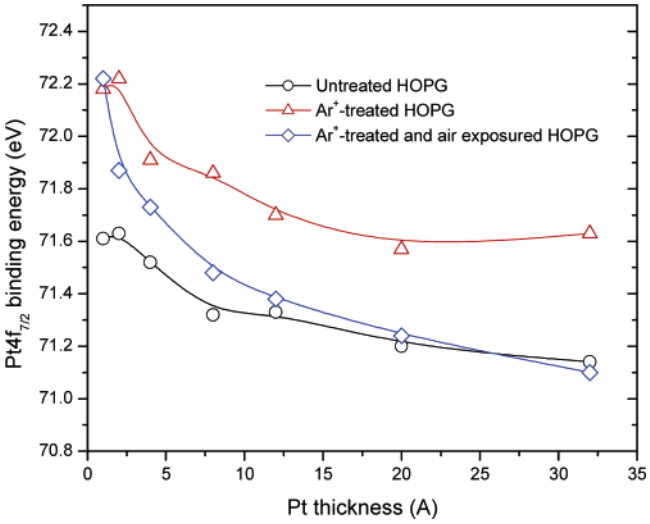

Figure 2. Binding energy shifts of the $Pt4f_{7/2}$ spectra as a function of Pt deposition onto variously treated HOPG surfaces.

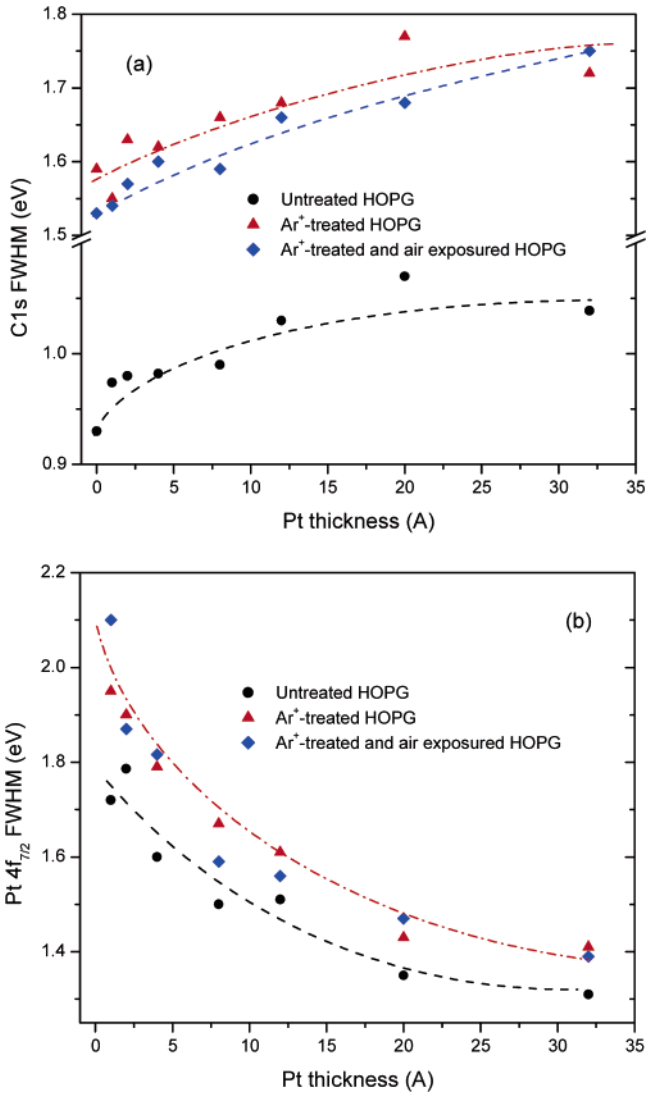

Figure 3. Fwhm changes of the (a) C1s and (b) $Pt4f_{7/2}$ spectra as a function of Pt deposition onto variously treated HOPG surfaces.

by an excitonic state near the Fermi level (π-electron band) in the hole-state density of states,[48] due to many-electron effects, although an alternative view, using attributable, quantifiable, overlapping symmetric peak components, exists.[44]

All C1s and $Pt4f_{7/2}$ spectra could be fit with asymmetry line shapes having appropriate asymmetry parameters. Typical C1s and Pt4f spectra, and their asymmetric peak fits, are seen in Figure 1, after Shirley background subtraction. The peak binding energies are seen in Figure 2, as a function of Pt thickness, as are the fwhm's in Figure 3, and the TS and TL asymmetry indices in Figure 4. As previously indicated,[44] the α asymmetry index varies linearly with the TS asymmetry index; this is confirmed in the present work, where, as shown in Figure 5, this relationship holds, regardless of HOPG surface treatment and Pt particle size.

We also found that each of the asymmetric Pt4f spin−orbit components may be fit with several symmetric peaks. While this was previously observed for Pt nanoparticles on SiO_2,[9] it was attributed there to many-electron effects, due to the particles being nonmetallic. We will report on our use of symmetric Pt peak components in a later paper.

The α asymmetry index of the C1s spectrum is seen to decrease (Figure 4), and its fwhm to increase (Figure 3), with increasing Pt thickness, while those of Pt change in the opposite directions. These changes are accompanied by (1) an increase in C1s intensity (Figure 6) over the first 0.5 nm of Pt deposition, before a decrease with further deposition, and (2) a slight increase in C1s binding energy (not shown) over the same first 0.5 nm of Pt thickness.

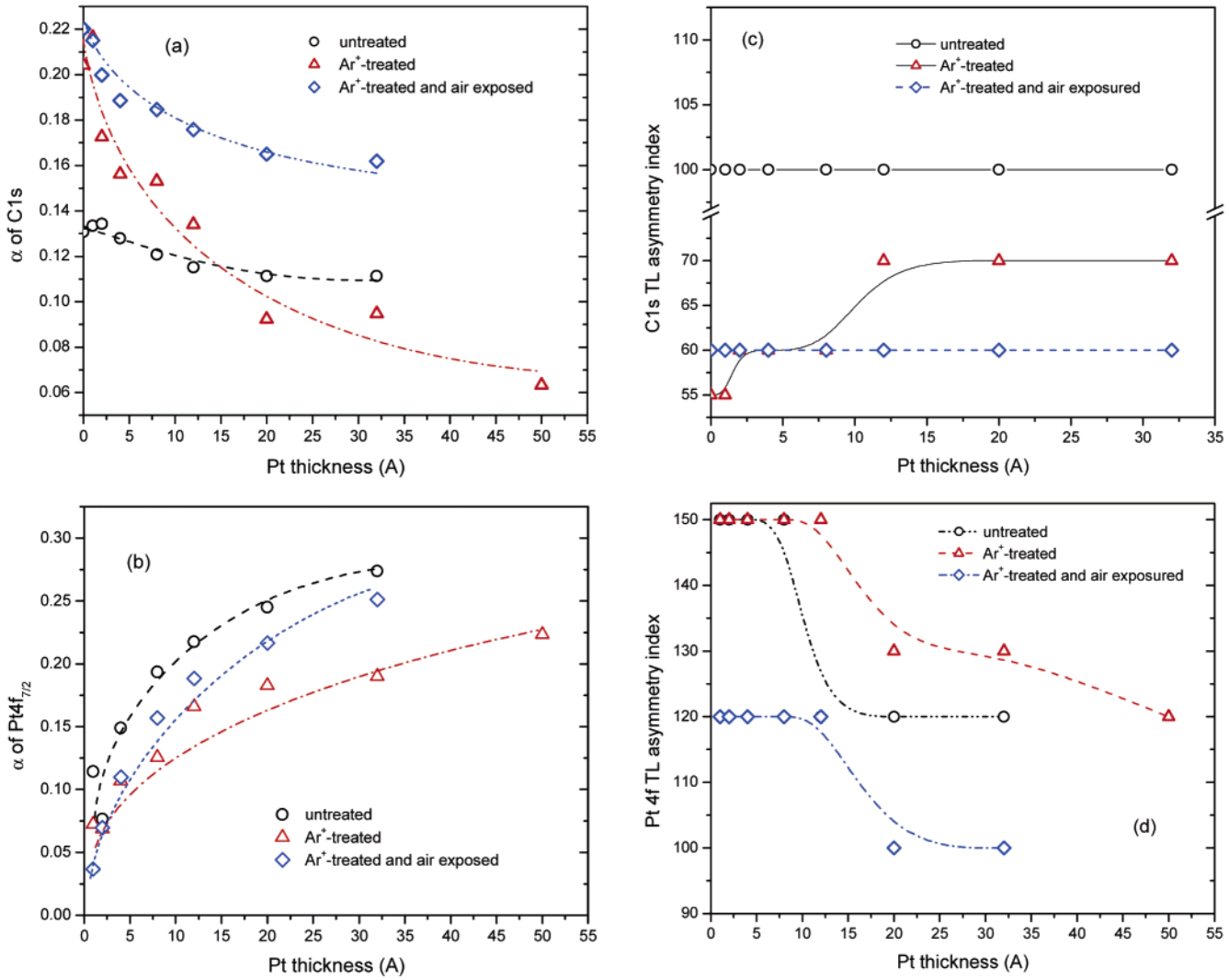

Figure 4. Asymmetry indices as a function of Pt deposition onto variously treated HOPG surfaces: α indices for (a) C1s and (b) $Pt4f_{7/2}$; TL indices for (c) C1s and (d) $Pt4f_{7/2}$.

The TL indices for untreated and for air-exposed Ar^+-treated HOPG do not seem to change with Pt deposition, although those for Ar^+-treated (not air-exposed) HOPG increase. As we previously showed,[18] this latter treatment produces stable free radicals in this spectral region, which are shown by the TL values and their effect on the C1s peak asymmetry.

The changes in the TL indices for Pt, under all conditions, are clearly size-related. They may be associated with the dimensions of the Kubo gap, which is the average energy of the gap between quantum levels at the Fermi energy: while normally much less than *kT* for a metal, the gap increases in size as the particle dimension decreases, eventually becoming greater than *kT*. At this point, the particle becomes nonmetallic. This occurs in the 1−2 nm range.[54]

Thus, the asymmetry parameters, peak positions (particularly that of $Pt4f_{7/2}$), peak widths, and C1s peak intensity are all dependent on the nominal thickness of deposited Pt. The changes in the $Pt4f_{7/2}$ spectrum, with increasing Pt deposition thickness, are due to contributions from nanoparticle/substrate interactions[15,16] and size-dependent final-state effects,[9] without the formation of Pt−C covalent bonds (no carbide formation).

The fwhm values for both the $Pt4f_{7/2}$ and C1s spectra (Figure 3) manifest different developments with deposition: $Pt4f_{7/2}$ shows a continued decrease and C1s a continued increase. Although the $Pt4f_{7/2}$ spectrum contains contributions from both the nanoparticle size and its interaction with the substrate, which are difficult to separate, this does not apply to the C1s spectrum. The increase of the C1s fwhm (Figure 3a), due to phonon broadening, indicates that there is *some* interaction between Pt and the HOPG surface, whether or not the surface is treated. Added to the decrease seen in the C1s asymmetry index, these observations suggest that the charge transfer from the Pt particle to the HOPG surface, or localized surface electron states, is partly compensated (perturbed) by the Pt particles. This is more clearly seen for a more localized surface, such as that for Ar^+-treated HOPG, in Figure 4a, due the increased interaction between Pt and HOPG.

The normalized C1s peak area, as a function of Pt deposition (Figure 6), varies in a manner similar to that of Ni nanoparticles on HOPG,[21] with the enhanced photoemission from the substrate attributed to the forward scattering of photoelectron diffraction through the Pt:[55] the forward scattering of the photoelectrons aligns as the initial nanoparticle size increases and the crystallinity and orientation are perfected;[55−57] again, this indicates interfacial interaction insofar as the ability to orient the direction of crystalline perfection with respect to the plane of the substrate. Eventually, orientational order is lost with increasing size, and scattering increases.

Decreases of the C1s asymmetry indices with Pt deposition, especially for Ar^+-treated HOPG, with simultaneous increases

TABLE 1: C1s Asymmetry Parameter Analysis from the Variously Treated HOPG Surfaces

surface	fwhm (eV)	TS asymmetry index	α asymmetry index	oxygen concn (atom %)
untreated	0.93	0.17	0.135	<1
Ar^+-treated	1.59	0.30	0.206	0
Ar^+-treated and air-exposed	1.53	0.30	0.214	~10

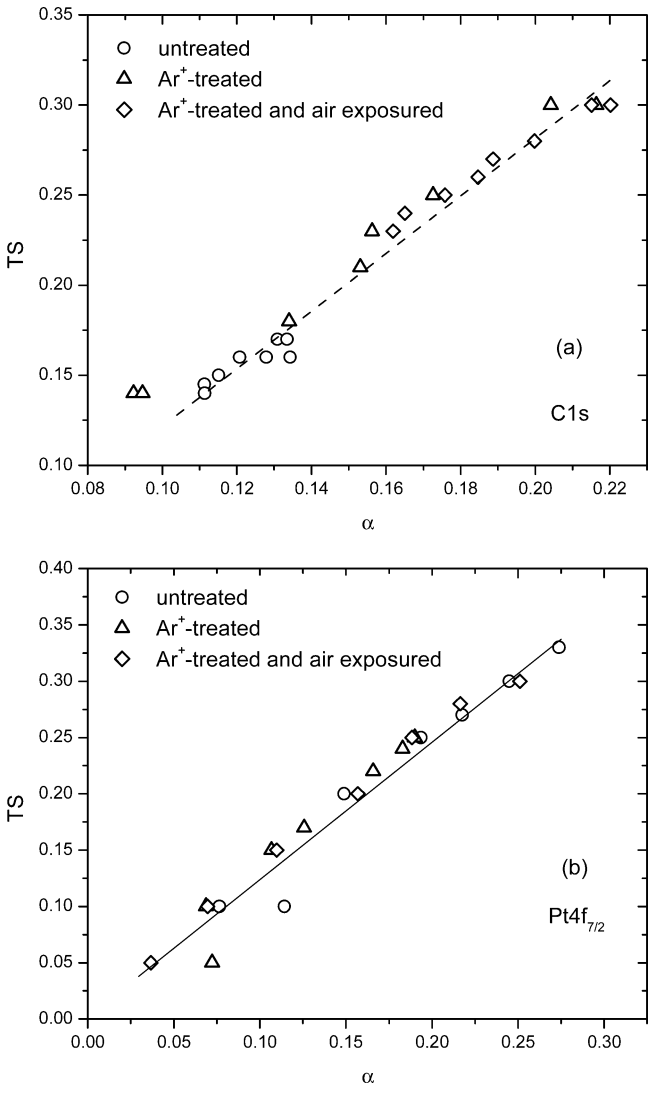

Figure 5. TS asymmetry indices as a function of α: (a) C1s, (b) $Pt4f_{7/2}$.

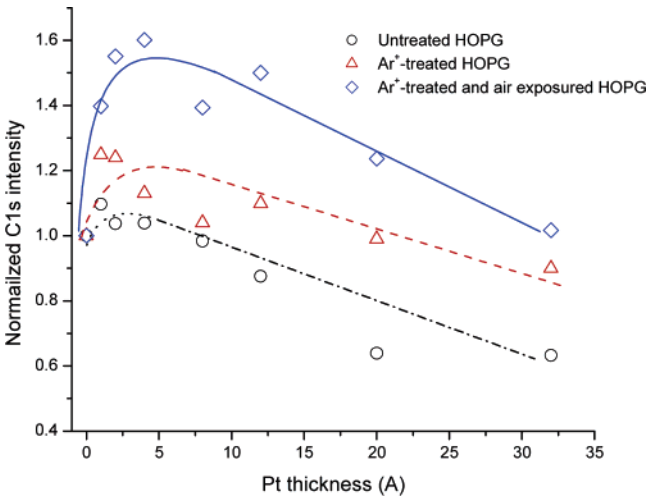

Figure 6. Normalized C1s peak intensity as a function of Pt deposition onto variously treated HOPG surfaces.

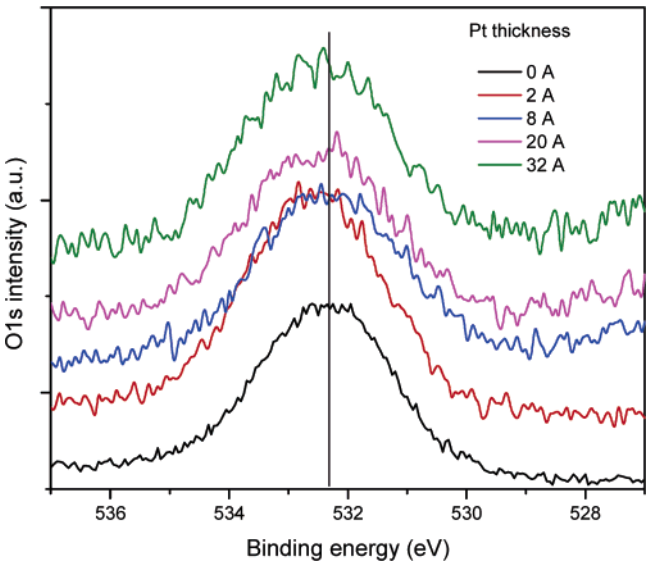

Figure 7. O1s spectral evolution on the Ar^+-treated and air-exposed HOPG surface as a function of Pt deposition.

of the $Pt4f_{7/2}$ asymmetry indices, also indicate interfacial interaction. All these change patterns in our C1s and $Pt4f_{7/2}$ spectral features, occurring upon Pt deposition, are similar to those in an early report on Pt deposited onto carbon foil,[7] although they were attributed to another source.

While the free radicals, created at the HOPG surface on Ar^+ treatment, react readily with O_2 and H_2O on air exposure, which can lead to a significant increase in the relative concentration of incorporated oxygen, this causes a minor change in the C1s α peak asymmetry index, from 0.206 on Ar^+ treatment to 0.214 (Table 1). The O1s evolution on Pt deposition onto an air-exposed Ar^+-treated HOPG surface is seen in Figure 7. Although there is a slight broadening of the line width, there is a lack of any firm evidence of the formation of a Pt−O bond (a new component would be expected in the 530−531 eV range, and might be difficult to see because of the weak signal).

The time-dependent stabilities of the C1s and $Pt4f_{7/2}$ spectra offer insights into nanoparticle/interface interactions. Figure 8a shows the time dependence of the C1s peak area intensity of a nominal monolayer of Pt deposited onto variously treated HOPG substrates, and Figure 8b shows the corresponding $Pt4f_{7/2}$ dependence. In all cases, the C1s spectra are characterized by an initial decrease in intensity over the first moments after deposition, followed by an increase over the initial 10 min; this is followed by a slower decrease over the next 2 h. As the $Pt4f_{7/2}$:C1s ratio in Figure 9 shows, there is no change, as a function of time, beyond the first few minutes of nanocrystal reorganization, indicating an absence of coalescence; that is, the nanoparticles are fixed to the surface.

The $Pt4f_{7/2}$ spectra do not show the initial decrease in intensity seen in the C1s spectra but mirror the increase and the subsequent decrease. Similar behavior characterizes the α asymmetry indices in Figure 10, although with more scatter. The initial decrease in the C1s spectra implies a time-dependent interfacial alignment in the Pt nanoparticle (chemical reactions

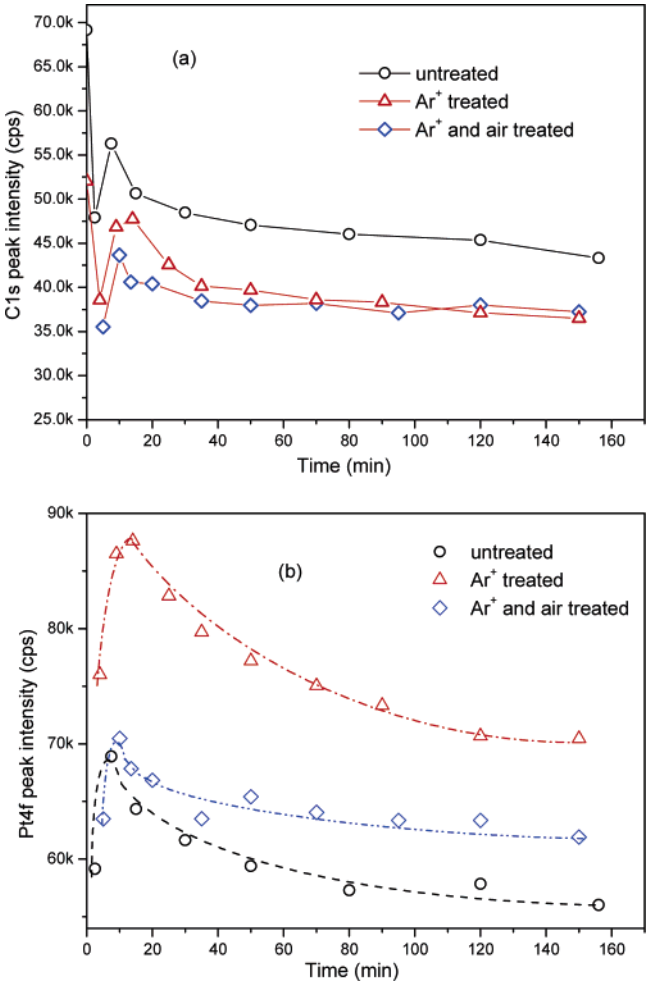

Figure 8. Peak intensity changes of the (a) C1s and (b) Pt4f$_{7/2}$ spectra as a function of time for 0.3 nm Pt deposited onto variously treated HOPG surfaces.

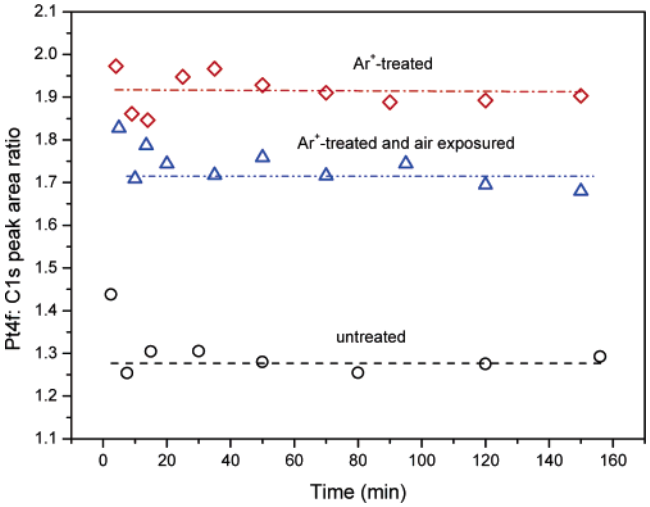

Figure 9. Pt4f$_{7/2}$:C1s intensity ratio as a function of time for 0.3 nm Pt deposited onto variously treated HOPG surfaces.

would be expected to occur far more quickly), and coalescence is ruled out because of strong adhesion;[58] once this occurs, the time-dependent behaviors of both spectra are quite similar, indicating an increased forward scattering due to Pt nanocrystalline alignment, followed by a crystalline reorganization.

Such a reorganization is demonstrated by the high-resolution electron microscopy sequence seen in Figure 11. It is but one sequence coming from nominal 0.1 nm thick samples of Pt,

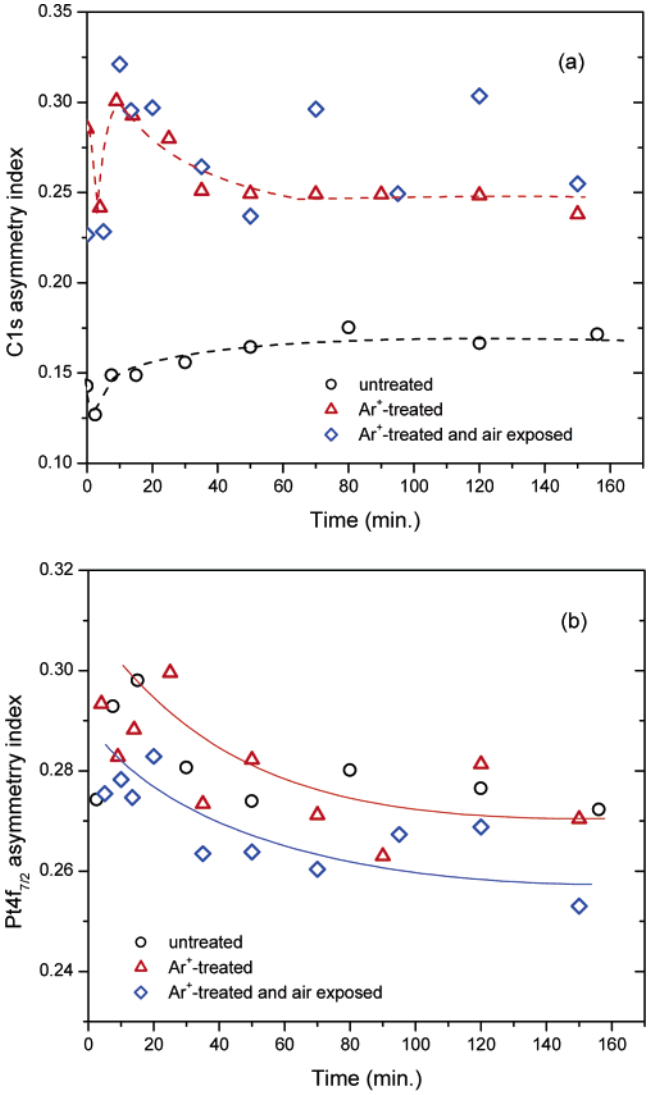

Figure 10. Time-dependent α asymmetry indices of (a) C1s and (b) Pt4f$_{7/2}$ spectra for 0.3 nm Pt deposited onto variously treated HOPG surfaces. As indicated in the text, the α indices vary in a manner identical to that of the TS indices, and may be used interchangeably.

evaporated onto freshly cleaved HOPG, and held at 450 °C, a temperature essential to supply the energy necessary for the reorganization to be seen over a longer period of time; there is a period of about 5 s between each frame. The evolution is characterized by (1) a Pt particle size distribution from ~1 to 2.5 nm, with well-defined, oriented crystals after the initial stage of nucleation and growth, (2) a lack of motion across the HOPG surface, even at 450 °C, obviating coalescence, in agreement with the XPS data, and (3) changes in the crystalline structure, as demonstrated by the continually changing fast Fourier transforms, inserted as the corresponding electron diffraction patterns.

Discussion

Interaction of Pt Nanoparticles with the HOPG Surface. For the three treatments used here, the Pt4f$_{7/2}$ peak shifts to lower binding energy (Figure 2b) and its fwhm narrows (Figure 3b) with increasing Pt deposition, consistent with the behavior of Pt nanoparticles supported on SiO_2.[9] This can be attributed to nanoparticle size-dependent (final-state) effects and phonon broadening, as well as broadening induced by inhomogeneities in the nanoparticles. This behavior is similar to that of many

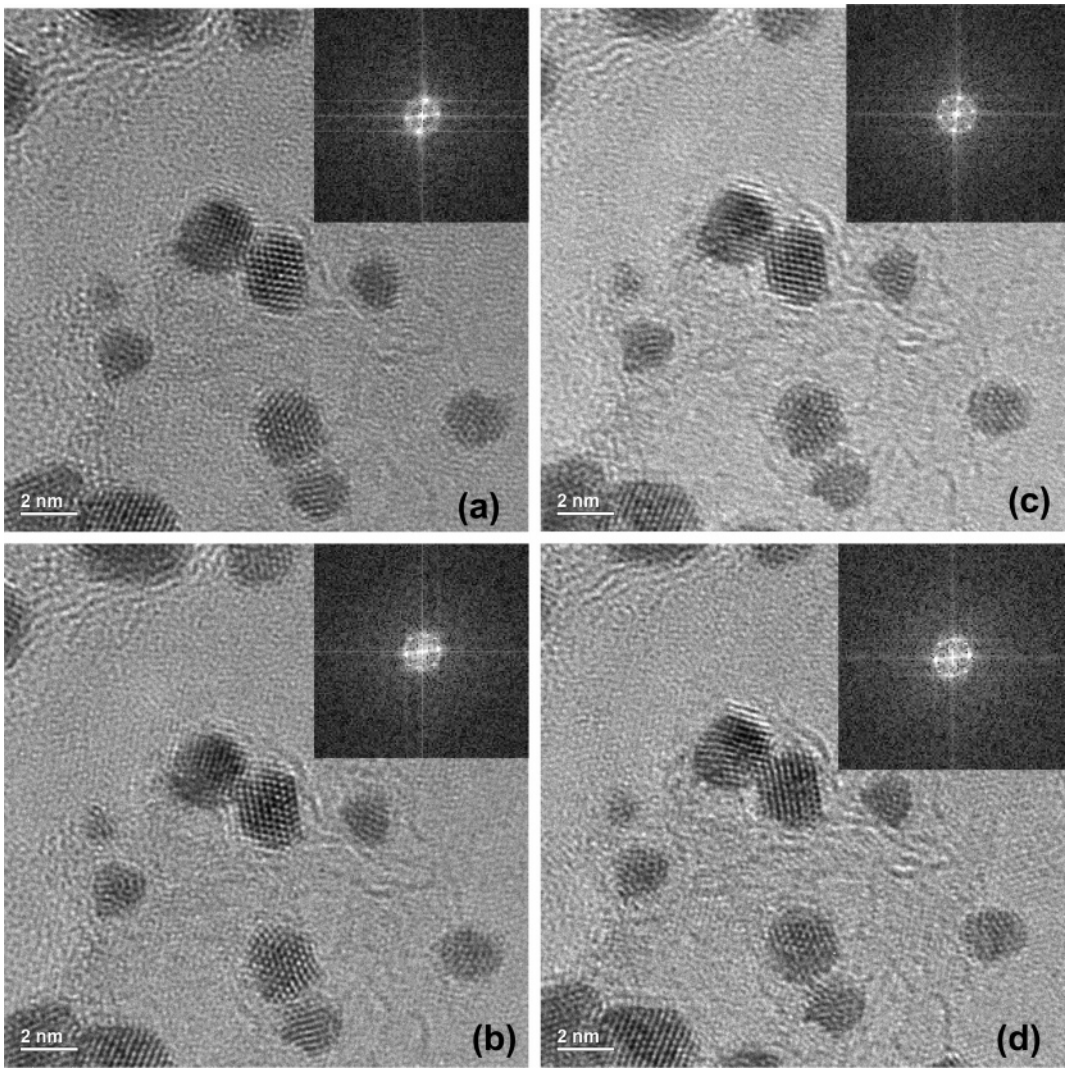

Figure 11. A sequence of HREM photomicrographs of Pt nanoparticles evaporated onto untreated HOPG, taken at 5 s intervals at 450 °C. The insets to each photomicrograph are the fast Fourier transforms of the diffraction patterns.

other deposited nanoparticles. Judging from the binding energy shifts, their known relationship to nanoparticle sizes, and the known relationship of nanoparticle size to nanoparticle/substrate interaction, we conclude that the interaction of Pt nanoparticles with the substrates used here is in the order Ar^+-treated > Ar^+-treated and air-exposed > untreated. The increase of the C1s fwhm (Figure 3a) and the decrease of the α and TS asymmetry indices with increasing Pt deposition indicate phonon broadening and charge transfer from Pt particles to the HOPG surface induced by interfacial reaction.

The α asymmetry index (which we have shown[44] to behave identically to the TS asymmetry index; see also Figure 5) is generally associated with the Pt nanoparticle size.[7,9] The behavior of the TS indices, in Figure 4b, indicates that the Pt nanoparticles deposited onto our samples have the size order Ar^+-treated < Ar^+-treated and air-exposed < untreated, consistent with the conclusions previously drawn from the binding energy shifts.

The C1s line shape undergoes significant changes induced by Pt deposition. The fwhm increases (Figure 3a), and the asymmetry index decreases (Figure 4a), with increasing Pt deposition. The decrease of the asymmetry index is a result of a decrease in the C2 component of the C1s spectrum,[44] due to localized (damaged) electron delocalization, and signals that the presence of Pt nanoparticles at these defects heals the previously localized electron delocalization, probably through interfacial interaction. The increase of fwhm with Pt deposition is most probably due to phonon broadening, due to this interfacial interaction. The order of TS asymmetry index values (Figure 4a) implies that the ability to mend the damaged HOPG surface structure is in the order Ar^+-treated and air-exposed > Ar^+-treated > untreated, while the order of the fwhm values (Figure 3a) is that previously found for Pt: Ar^+-treated > Ar^+-treated and air-exposed > untreated.

The electronic configuration of zerovalent Pt is [Xe] d^{10}, with no unpaired electrons. Its interaction with HOPG would then be expected to be similar to that of Ni, which forms back-bonds to defects in the HOPG surface.[21] Indeed, as STM data[14] show, Pt initially nucleates along steps of the untreated HOPG surface, which contain defects, and does not diffuse laterally;[58] this is similar to the behavior of Ni.[21] The introduction of defects by Ar^+ treatment increases the surface density of bonding sites, resulting in a higher density of smaller Pt nanoparticles.[58] The reaction of Pt nanoparticles with an Ar^+-treated surface that has been exposed to air has previously been shown[58] to be chemical in nature, with hydrogen bonds formed between the oxidized HOPG surface and the surface-oxidized Pt nanoparticle. The unexpected order of Pt nanoparticle interaction with the treated HOPG substrates (i.e., Ar^+-treated > Ar^+-treated and air-exposed, as revealed by our studies) reflects the stronger

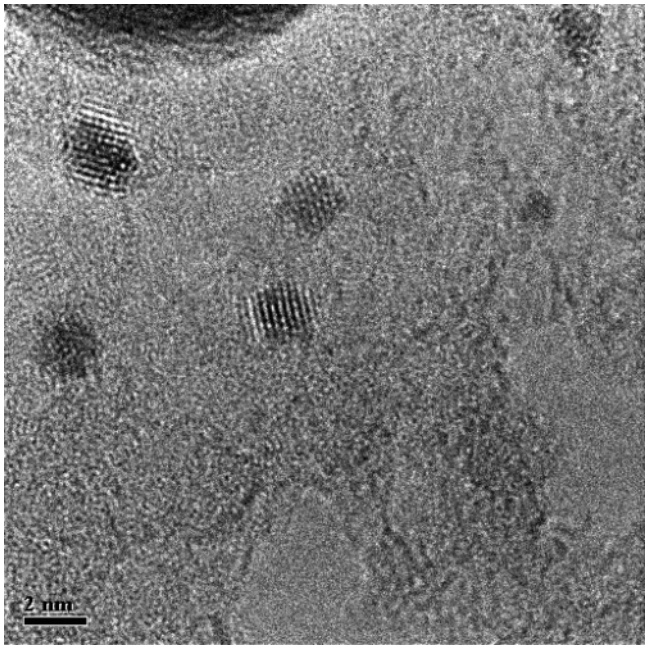

Figure 12. An HREM photomicrograph of a HOPG surface containing Pt nanoparticles, after 2 h of C^+ perpendicular irradiation at 2 MeV. The nanoparticles have moved on irradiation, their shapes have been modified, and the presence of a moiré pattern gives evidence for graphene layer damage and rotation.

bonds formed on Pt back-bonding to HOPG free radical defects, introduced on Ar^+ treatment, than their reaction with the chemical species subsequently introduced on air exposure. These results are consistent with very recent SEM results[59] for Au nanoparticles evaporated onto Ar^+-treated HOPG and amorphous carbon (which is similar to Ar^+ treatment followed by air exposure): the Au nanoparticle size on Ar^+-treated HOPG was found to be smaller than that on amorphous carbon when similar thicknesses were deposited at room temperature.

B. Reorganization of Pt Nanoparticle Crystallinity on the HOPG Surface. The variation of the C1s peak intensity with deposition thickness (Figure 6) and with time (Figure 8a), as well as that of the $Pt4f_{7/2}$ peak with time (Figure 8b), points to changes in the crystalline structure of the Pt nanoparticles while remaining fixed to the substrate. Figure 11 demonstrates such crystallinity changes in Pt nanoparticles. The conditions used were different from those for our XPS observations, in that thermal energy was continually supplied; this was made necessary so as to permit HREM observations over the longer time scale necessitated by sample preparation and insertion into the electron microscope.

We believe that the reorganization is simply the particle shape oscillations we spoke of in our previous paper,[60] described by the Frank−Read slip mechanism, here modified by the nanoparticle/substrate interaction already identified in the present work. The energy for this derives from the condensation energy of the Pt nanoparticle (~565 kJ/mol), which, until it dissipates into the surroundings, serves to orient the entire nanoparticle; the dissipation time found here is of the same order of magnitude as the time previously found for energy dissipation from Cu nanoparticles after low-energy ion bombardment.[61] Once dissipated, the thermal background permits the Frank−Read mechanism to produce sufficient distortions to randomize the crystalline orientation with respect to the surface.

The concept of crystalline orientation through energy dissipation is supported by our recent study of the irradiation of Pt nanoparticles in a 2 MeV Pelletron accelerator, using a perpendicular C^+ beam at a flux of 3×10^{15} (ions/cm^2)/s; the beam energy is transferred to the Pt nanoparticles through electron stopping. This energy was used to affect motion and crystalline modifications in the nanoparticles, causing noticeable damage to the substrate, before being transferred to the HOPG. By contrast, we have found that the identical irradiation of clean HOPG has little effect, even after 2 h. The presence of Pt nanoparticles is thus the intermediary for the production of substantial changes: (1) the nanoparticles move during irradiation, as energy from the beam is transferred to the Pt and dissipated to the substrate in movement, as previously found;[60] (2) such energy transfer to the substrate leads to damage and rotation in the outer layers of the HOPG, as evidenced by the moiré patterns that appear. Figure 12 shows the results of 2 h of C^+ irradiation; a more detailed account will be published elsewhere.

Conclusions

A systematic XPS core-level asymmetry index analysis has been used to characterize Pt nanoparticles on variously treated HOPG surfaces. Our analysis, based on both the size-dependent $Pt4f_{7/2}$ and size-independent C1s spectral features (binding energy shift, fwhm, and asymmetry indices), indicates that Pt nanoparticles interact most extensively with the Ar^+-treated HOPG surface, and least extensively with the untreated HOPG surface. In all cases, the reaction is sufficiently extensive to bind the Pt nanoparticles and to permit the observation of a crystalline reorganization during the dissipation of the heat of condensation into the surroundings.

Acknowledgment. We thank the Natural Sciences and Engineering Research Council of Canada, GM Canada, the Welch Foundation, and the International Center for Nanotechnology and Advanced Materials for funding.

References and Notes

(1) Henry, C. R. *Surf. Sci.* **1998**, *31*, 231.
(2) Binns, C.; Baker, S. H.; Demangeat, C.; Parlebas, J. C. *Surf. Sci.* **1999**, *34*, 105.
(3) Freund, H.-J. *Surf. Sci.* **2002**, *500*, 271.
(4) Gates, B. C. *J. Mol. Catal. A* **2000**, *163*, 55.
(5) Antolini, C. *J. Mater. Sci.* **2003**, *38*, 2995.
(6) Mason, M. G.; Gerenser, L. J.; Lee, S. T. *Phys. Rev. Lett.* **1977**, *39*, 28.
(7) Cheung, T. T. *Surf. Sci.* **1984**, *140*, 151.
(8) Murgai, V.; Raaen, S.; Strongin, M.; Garrett, R. F. *Phys. Rev. B* **1986**, *33*, 4345.
(9) Eberhardt, W.; Fayet, P. *Phys. Rev. Lett.* **1990**, *64*, 780.
(10) Steve, C.; Chottiner, G. S.; Scherson, D. A.; Pruett, G. *Langmuir* **1990**, *6*, 1316.
(11) Schmidt, A. A.; Eggers, H.; Herwig, K.; Anton, R. *Surf. Sci.* **1996**, *349*, 301
(12) Marcus, P.; Hinnen, C. *Surf. Sci.* **1997**, *392*, 134.
(13) Zoval, J. V.; Lee, J.; Gorer, S.; Penner, R. M. *J. Phys. Chem. B* **1998**, *102*, 1166.
(14) Howells, A. R.; Hung, L.; Chottiner, G. S.; Scherson, D. A. *Solid State Ionics* **2002**, *150*, 53.
(15) Fauth, K.; Hessler, M.; Batchelor, D.; Schütz, G. *Surf. Sci.* **2003**, *529*, 397.
(16) Fauth, K.; Schneider, N.; Hessler, M.; Schütz, G. *Eur. Phys. J. D* **2004**, *29*, 57.
(17) Rheaume, J. M.; Müller, B.; Schulze, M. *J. Power Sources* **1998**, *76*, 60.
(18) Yang, D.-Q.; Sacher, E. *Surf. Sci.* **2002**, *504*, 125.
(19) Yang, D.-Q.; Sacher, E. *Surf. Sci.* **2002**, *516*, 43.
(20) Engelhard, M.; Baer, D. *Surf. Sci. Spectra* **2000**, *7*, 1.
(21) Yang, D.-Q.; Sacher, E. *J. Phys. Chem. B* **2005**, *109*, 19329.
(22) Roy, H.-V.; Fayet, P.; Patthey, F.; Schneider, W.-D.; Delley, B.; Massobrio, C. *Phys. Rev. B* **1994**, *49*, 5611.
(23) Mahan, G. D. *Phys. Rev.* **1967**, *163*, 612.
(24) Nozières, P.; de Domenicis, C. T. *Phys. Rev.* **1969**, *178*, 1097.
(25) Doniach, Šunjic, M. *J. Phys. C: Solid State Phys.* **1970**, *3*, 285.

(26) Gadzuk, W.; Šunjic, M. *Phys. Rev. B* **1975**, *12*, 524.
(27) Anderson, P. W. *Phys. Rev. Lett.* **1967**, *18*, 1049.
(28) Hüfner, S.; Wertheim, G. K. *Phys. Rev. B* **1975**, *11*, 678.
(29) Chiang, S.; Wertheim, G. K.; Di Salvo, F. J. *Solid State Commun.* **1976**, *19*, 75.
(30) Shevchik, N. J. *Phys. Rev. Lett.* **1974**, *33*, 1336.
(31) Dow, J. D.; Franceschetti, D. R. *Phys. Rev. Lett.* **1975**, *34*, 1320. This reference also contains a substantial list of previously published papers challenging the validity of the Mahan process and its application to XPS.
(32) Citrin, P. H. *Phys. Rev. B* **1973**, *8*, 5545.
(33) Hüfner, S.; Wertheim, G. K.; Buchanan, D. N. E. *Chem. Phys. Lett.* **1974**, *24*, 527.
(34) Hüfner, S.; Wertheim, G. K. *Phys. Lett. A* **1975**, *51*, 301
(35) Hüfner, S.; Wertheim, G. K.; Wernick, J. H. *Solid State Commun.* **1975**, *17*, 417.
(36) Wertheim, G. K.; Hüfner, S. *Phys. Rev. Lett.* **1975**, *35*, 53.
(37) Citrin, P. H.; Wertheim, G. K.; Baer, Y. *Phys. Rev. Lett.* **1975**, *35*, 885.
(38) Wertheim, G. K.; Walker, L. R. *J. Phys. F: Met. Phys.* **1976**, *6*, 2297.
(39) Wertheim, G. K. *Phys. Rev. B* **1982**, *25*, 1987.
(40) Minnhagen, P. *Phys. Lett. A* **1976**, *56*, 327.
(41) McManus, M. K.; Cochrane, R. W.; Sacher, E. Unpublished results.
(42) *Gmelin's Handbuch der Anorganischen Chemie*, Kobalt, Teil A Ergäzungsband, Achte Auflage; System-Nummer 58; Verlag Chemie: Weinheim, Germany, 1961; p 34.
(43) Yang, D.-Q.; Sacher, E. Unpublished results.
(44) Yang, D.-Q.; Sacher, E. *Langmuir* **2006**, *22*, 860.
(45) http://www.phy.cuhk.edu.hk/~surface/XPSPEAK/.
(46) Yang, D.-Q.; Poulin, S.; Sacher, E.; Hyett, C. *Appl. Surf. Sci.* **2000**, *165*, 116.
(47) Yang, D.-Q.; Sacher, E. *Appl. Surf. Sci.* **2001**, *173*, 30.
(48) P. M. Th. M. van Attekum, Wertheim, G. K. *Phys. Rev. Lett.* **1979**, *43*, 1896.
(49) Cheung, T. T. P. *J. Appl. Phys.* **1982**, *53*, 6857;
(50) Cheung, T. T. P. *J. Appl. Phys.* **1984**, *55*, 1388
(51) Prince, K. C.; Ulrych, I.; Peloi, M.; Ressel, B.; Cháb, V.; Crotti, C.; Comicioli, C. *Phys. Rev.* **2000**, *62*, 6866.
(52) Sette, F.; Wertheim, G. K.; Ma, Y.; Meigs, G.; Modesti, S.; Chen, C. T. *Phys. Rev. B* **1990**, *41*, 9766.
(53) Śmith, R. A.; Armstrong, C. W.; Smith, G. C.; Weightman, P. *Phys. Rev. B* **2002**, *66*, 245409.
(54) Rao, C. N. R.; Kulkarni, G. U.; Thomas, P. J.; Edwards, P. P. *Chem.—Eur. J.* **2002**, *8*, 28.
(55) Egelhoff, W. F., Jr. *Phys. Rev. B* **1982**, *30*, 1052; *J. Vac. Sci. Technol., A* **1985**, *3*, 1511.
(56) Armstrong, R. A.; Egelhoff, W. F.; Jr. *Surf. Sci.* **1985**, *154*, L225.
(57) Yang, D.-Q.; Sun, Y.; Da, D. A. *Appl. Surf. Sci.* **1999**, *144−145*, 451.
(58) Yang, D.-Q.; Sacher, E. *Chem. Mater.* **2006**, *18*, 1181.
(59) Büttner, M.; Oelhafen, P. *Surf. Sci.* **2006**, *600*, 1170.
(60) José-Yacamán, M.; Gutierrez-Wing, C.; Miki, M.; Yang, D.-Q.; Piyakis, K. N.; Sacher, E. *J. Phys. Chem. B* **2005**, *109*, 9703.
(61) Yang, D.-Q.; Sacher, E. *Surf. Sci.* **2003**, *536*, 67.